

# Cyclic Stress-strain Data Analysis Under Biaxial Tensile Stress State

by A. Zouani, T. Bui-Quoc and M. Bernard

**ABSTRACT**—A new device was developed to assess fatigue life under biaxial tensile loading at elevated temperatures. It makes use of an annular disk specimen and can be easily mounted onto a standard push-pull machine so that the axial force is converted into radial forces extending across the disk specimen. Therefore, a positive ratio of the tangential to the radial stress can be imposed at the reduced section of the disk specimen; this ratio depends on the specimen configuration and may be fixed to a value ranging from 0.5 to 0.9 by varying the inner diameter of the disk. The proposed device has performed successfully and was used to study the cyclic behavior of Type-304 stainless steel subjected to various biaxial tensile stress states at room temperature and at 200°C. The data obtained from this experimental procedure have been analyzed to evaluate the effectiveness of some correlations already available for treating the biaxial cyclic stress-strain response in terms of the uniaxial behavior. This analysis shows that a successful correlation should account for all the stress components. The authors discuss the concept used in the modeling of the material cyclic behavior and the formulation of a biaxial fatigue damage parameter necessary for an effective analytical life prediction methodology.

## Nomenclature

$a$  = characteristic radial length in the gage section of the disk specimen  
 $E$  = elastic modulus  
 $F, F_1, F_2$  = axial loads  
 $K, K'$  = monotonic and cyclic strain-hardening coefficients  
 $M_b$  = bending moment  
 $M_t$  = torsion moment  
 $n, n'$  = monotonic and cyclic strain-hardening exponents  
 $P$  = internal/external pressure  
 $R$  = load ratio (ratio between the minimum and maximum applied load)  
 $R_b$  = disk bore radius  
 $(r, \theta, z)$  = cylindrical coordinates  
 $T$  = test temperature  
 $x$  = radial distance from the center of the gage section  
 $\epsilon_{eq}$  = von Mises equivalent strain  
 $\epsilon_r$  = radial strain

$\epsilon_\theta$  = tangential strain  
 $\epsilon_z$  = axial strain  
 $\gamma_{eq}$  = Tresca equivalent strain or maximum shear strain  
 $\nu$  = Poisson's ratio  
 $\rho$  = biaxial stress ratio ( $\rho = \sigma_\theta/\sigma_r$ )  
 $\sigma_1, \sigma_2$  = in-plane maximum and minimum principal stresses  
 $\sigma_{eq}$  = von Mises equivalent stress  
 $(\sigma_{Mises})_{max}$  = maximum von Mises stress in the specimen  
 $\sigma_r$  = radial stress  
 $\sigma_{rz}, \sigma_{\theta z}, \sigma_{xz}$  = shear stresses  
 $\sigma_\theta$  = tangential stress  
 $\sigma_u$  = ultimate tensile stress  
 $\sigma_x, \sigma_z$  = axial stress  
 $\sigma_y$  = yield stress  
 $\tau_{eq}$  = Tresca equivalent stress or maximum shear stress

## Introduction

For several in-service components, the constituent parts are usually subjected to complex loading that leads to multi-axial stress and strain fields at critical surface locations. Consequently, a reliable design procedure based on multi-axial experimental data is necessary to ensure a satisfactory performance over the predetermined service period. In fact, the lifetime assessment of a particular component requires knowledge of the cyclic stress-strain behavior and the fatigue properties under biaxial loading conditions. These properties can only be established on the basis of an experimental approach; for this reason, the development of testing equipment and measuring devices has been the driving force behind the advancement of the multi-axial fatigue research.

To better understand the fatigue behavior of gas turbine rotating parts, Zouani, Bui-Quoc and Bernard<sup>1</sup> initiated a research program for studying material cyclic behavior and developing a reliable fatigue life parameter under biaxial tensile cyclic loading at a relatively high temperature. For this purpose, a useful laboratory device was designed. It makes use of an annular disk specimen subjected to cyclic loading through a spatial-arms mechanism mounted on a standard servohydraulic testing machine. The design concept of this device and a brief review of the existing multi-axial testing methods were already published;<sup>1</sup> only a summary of this review is given in Appendix A. From this review, it is seen that the commonly used methods—that is, the thin-walled tube under internal/external pressure and axial load<sup>2</sup> and the cruciform specimen under biaxial tensile loading<sup>3</sup>—are suitable for achieving the objective in this study, but their applicability could not be easily made. The proposed device is viewed

A. Zouani is NSERC Fellow, Institute for Aerospace Research, National Research Council, Ottawa, Ontario, Canada K1A 0R6. T. Bui-Quoc and M. Bernard are Professors, Department of Mechanical Engineering, École Polytechnique de Montréal, Montréal, Québec, Canada H3C 3A7.

Original manuscript submitted: February 6, 1998.  
Final manuscript received: October 6, 1998.

as a simple and low-cost method that overcomes some difficulties related to the experimental techniques and responds adequately to the objective of the present research program.

Under biaxial loading conditions, some equivalent stress-strain relations are adopted to establish a correlation between the uniaxial and the biaxial results, since the fatigue material behavior is determined, in general, on the basis of uniaxial tests. The traditional approach uses either the Tresca or the von Mises stress-strain equivalents. Under biaxial proportional loading, Brown and Miller<sup>4</sup> concluded that a unique stress-strain curve could be determined for stable conditions by plotting the maximum shear stress in terms of the maximum shear strain. Doquet and Pineau<sup>5</sup> observed some deviations in the presentation of data obtained under in-phase tension and torsion tests when using Tresca and von Mises equivalents. Although some authors<sup>6</sup> emphasized the applicability of the von Mises concept, Bonacuse and Kalluri<sup>7</sup> reported that the von Mises equivalent predicts a stress-hardening effect under the torsional loading less than that exhibited by the material. The reason for this discrepancy is not yet known. The validity of such a relationship could only be examined by analyzing the results obtained for a wide range of the biaxial stress ratio.

The first part of this paper describes the new testing device and presents the preliminary tests carried out to ensure its good performance. The effectiveness of the von Mises and the Tresca concepts in treating the cyclic stress-strain data in terms of the uniaxial behavior is examined in the second part of this paper. For this purpose, the data recently obtained from Type-304 stainless steel tested under several biaxial tensile stress states at room temperature and at 200°C are used. The influence of the in-plane minor principal stress on the cyclic behavior is also emphasized.

## Testing Device

### Brief Description of the Testing Device

The proposed device, shown in Fig. 1, comprises a spatial-arms mechanism acting on an annular disk specimen with a reduced test section. The device is made up of four major parts: the upper and lower grips, the loading arms, the load transmitting plates and the disk specimen; a detailed description of the device may be found in Ref. 1. Essentially, the arms form two conical spiders arranged in such a way that once the upper and lower grip parts are moved toward each other, the compressive force generated by a conventional testing machine is converted into radial forces extending across the disk specimen. For this purpose, the outer ends of the loading arms are leaned (through the load-transmitting plates) against a shoulder machined along the disk specimen perimeter and the inner ends are leaned on grooves machined in the grip parts; a total of 16 arms and load-transmitting plates are used in the device.

With the present device, a positive ratio ( $\rho$ ) of the tangential stress ( $\sigma_\theta$ ) to the radial stress ( $\sigma_r$ ) may be imposed at the center of the test section; this ratio depends on the specimen configuration and may be fixed to a value ranging from 0.5 to 0.9 by varying the inner diameter of the disk. The geometry of the specimen was determined following a parametric optimization process based on a well-defined design criterion using the stress components in the specimen obtained from finite element calculations.<sup>8</sup> Figure 2 shows the geometry of

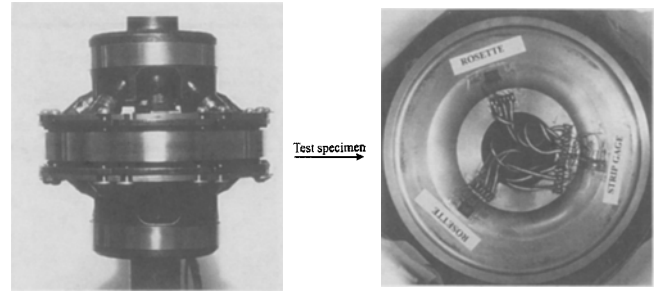


Fig. 1—Photograph of the fixture and a disk specimen with strain gages

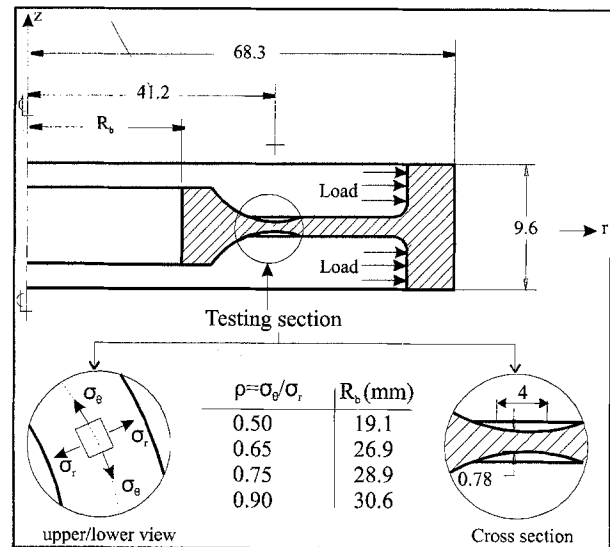


Fig. 2—Geometry of a typical disk specimen (dimensions in mm)

the disk specimen obtained using this process. As indicated in this figure, four bore radii ( $R_b$ ) were selected in order to impose four specific biaxial stress ratios ( $\rho = 0.5, 0.65, 0.75$  and  $0.9$ ) in the test section.

### Evaluation Tests

For evaluating the effectiveness of the proposed apparatus, preliminary biaxial static loading tests were carried out on disk specimens machined from an annealed Type-304 stainless steel; the chemical composition of this steel is given in Table 1. The uniaxial monotonic and cyclic properties, investigated through preliminary tests carried out on smooth cylindrical specimens with a diameter of 6.35 mm and a gage length of 25.4 mm, are reported in Table 2. The fatigue tests were conducted in accordance with ASTM Standard 606.

A specific disk specimen bore radius was selected ( $R_b = 19.1$  mm) so that a biaxial stress state associated with a stress ratio of 0.5 would be imposed in the test section. As illustrated in Fig. 1, two three-element 45-deg rosettes, having a gage length of 1.52 mm (type WA-06-060WR-120), and one strip gage, having a gage length of 1.57 mm and a centerline spacing of 2.03 mm (type EA-06-020MT-120), were cemented onto the upper specimen surface 120 deg from each other. The rosettes are used for simultaneous recording of the radial and the tangential strains in the reduced section of the specimen, whereas the strip gage measures the radial strain at

TABLE 1

C	Mn	P	S	Si	Cr	Ni	Mo	Cu	Co	N
0.02	1.66	0.029	0.021	0.49	18.28	8.70	0.90	0.56	0.112	0.072

TABLE 2

$E$ (GPa)	$\sigma_y$ (MPa)	$\sigma_u$ (MPa)	$n$	$K$ (MPa)	$n'$	$K'$ (MPa)
194	323	616	0.098	550	0.52	4520

different locations. Another three-element 45-deg rosette is cemented onto the lower surface of the specimen at a location opposite to the strip gage.

Figure 3 shows that the induced strains are practically uniform around the test section of the disk specimen. The strain gages located in this section give the values of the radial strain ( $\epsilon_r$ ) within a maximum deviation of 5 percent of each other. The maximum deviation between the measured tangential strains ( $\epsilon_\theta$ ) is less than 7 percent. Although an extensive investigation on the strain measurements focused on the upper surface of the test section, the results from the rosette mounted on the lower surface confirm that the bending effect is almost negligible as compared to the radial loading effect; the maximum deviation between the strains measured on both sides of the specimen is less than 10 percent.

The measured radial strains through the test section, illustrated in Fig. 4, show that the critical stress (or strain) location occurs at the thinnest test section. Moreover, over a region of  $a/2$  ( $a = 4.5$  mm) across the critical section in the radial

direction, the strain field is almost uniform, with a maximum deviation of 7 percent with respect to the average value in this area.

The dashed and dotted lines in Fig. 3 and the solid line in Fig. 4 represent the results obtained from a finite element analysis of the disk specimen; an axisymmetric model of the disk specimen was considered in the analysis together with the monotonic stress-strain data of the material. The finite element results are in reasonable agreement with experimental data; the maximum deviation of the calculated from the measured values is 10 percent for both the radial and the tangential strains. This agreement indicates that the strain distribution in the specimen is nearly axisymmetric and that the finite element model is appropriate for further investigation of the strain state in the test section of the disk specimen.

Figure 5 shows the measured tangential and radial strains in the test section under different load levels. It is seen that there is a linear relation between the measured tangential and radial strains due to the linear elastic behavior of the material. The value of the slope of the tangential strain–radial strain curve (equal to 0.2) is identical to the value of the biaxial strain ratio determined from the elastic stress-strain relationship using a biaxial stress ratio of 0.5. It is expected that there will be a deviation from the tangential strain–radial strain linear curve if large plastic strains are involved. For this reason, when investigating fatigue life in the low-cycle regime (with important plastic strains) under load control conditions, the imposed biaxial stress state was usually referred by the nominal biaxial stress ratio obtained in a linear elastic region. The latter parameter is independent of the applied load and the temperature levels. This characteristic value of the imposed stress state is very useful for engineering design purposes, since in most engineering applications the design of critical components is based mainly on the elastic analysis of the stress field.

From the results of preliminary evaluation tests, it is concluded that the proposed apparatus can produce a relatively large area of a uniform biaxial strain state. Moreover, with a limited number of loading-unloading cycles, applied manually to the disk specimen, the results have demonstrated a good repeatability of the strain measurements during cycling; that is, the same values of the strains have been recorded for a specific load level. These results confirm the potential of the proposed testing device to simulate a cyclic biaxial stress state with both stresses in tension.

### Investigation of the Biaxial Cyclic Behavior

The cyclic behavior of Type-304 stainless steel under biaxial tensile stress states was studied using the apparently convenient and economical multistep procedure. According to this procedure, the specimen was tested under a stepwise change of the load level until complete failure. At each step, cycling was carried out until the strains reached the stabilized

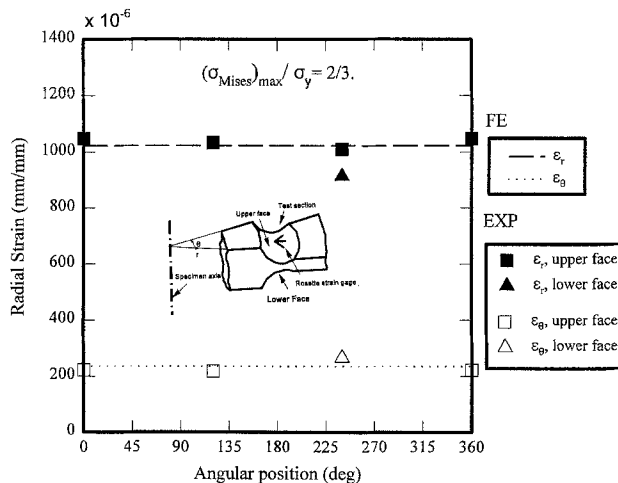


Fig. 3—Strain distribution in the test section along the circumferential direction

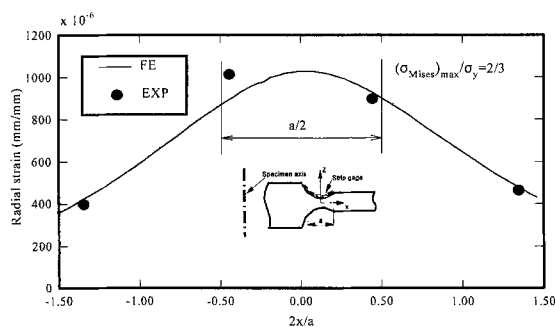


Fig. 4—Strain distribution in the test section along the radial direction

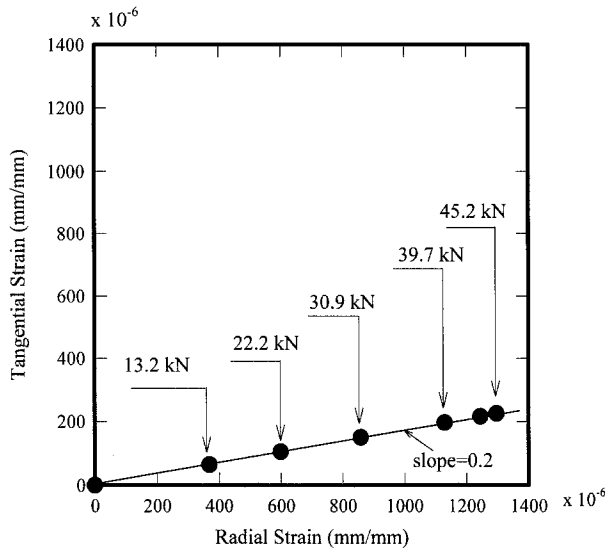


Fig. 5—Characteristic of the strain state in the test section under different load levels

conditions before switching to the next higher step. It should be noted that, under such a loading condition, a prior loading history has practically no influence on the stabilized cyclic behavior; this was observed on Type-316 stainless steel tested at different temperatures up to 600°C.<sup>9</sup>

### Experimental Procedure

The disk specimens were tested under multistep cyclic conditions at room temperature and at 200°C until complete rupture of the disk specimen. During a test, the applied load, the stroke, the radial and tangential strains in the test section and the number of applied cycles were stored periodically using a high-speed data acquisition system. The strains were measured by two rosette strain gages (similar to those used in the evaluation tests) cemented in the center of the test section 180 deg from each other. Four biaxial stress ratios equal to 0.5, 0.65, 0.75 and 0.9 were considered. The load signal was a triangular waveform under zero-to-tension condition ( $R = 0$ ,  $R$  being the ratio between the minimum and the maximum applied cyclic load) with a frequency of 0.1 Hz. Since the frequency was unchanged, the resulting stress rate depended on the load level.

For high-temperature testing, the test rig was located inside a furnace. A calibration was carried out to obtain a uniform temperature distribution in the area of the test section. For this purpose, six thermocouples were cemented onto the lower and upper faces of the test section 120 deg from each other. The measured temperatures indicate that the thermal gradient is almost negligible on each face; moreover, the maximum difference between the temperatures measured on both faces of the test section is less than 1 percent. It is noted that the high temperature considered in the present tests is limited by the performance of the high-temperature strain gages currently available.

### Results Analysis

Since the tests were carried out under load control conditions, the analysis is focused on the variation of the tangential and the radial strains in terms of the applied number of cycles.

Even though four different biaxial stress ratios were considered in the investigation, only those data obtained with the extreme values of this ratio (0.5 and 0.9) are emphasized. The other data are bounded between these two extreme cases.

### VARIATION OF PEAK STRAINS IN TERMS OF APPLIED CYCLES

The peak values of the radial and tangential strains are plotted in terms of the number of applied cycles in Fig. 6 for room temperature and in Fig. 7 for 200°C. Figures 6(a) and 7(a) correspond to  $\rho = 0.5$ , whereas Figs. 6(b) and 7(b) correspond to  $\rho = 0.9$ . From these figures, it is also seen that the biaxial strain ratio is not identical to that of the imposed stress ratio. In fact, the ratio between the radial strain and the tangential strain is in agreement with the value obtained under the assumption of an elastic stress-strain relationship for plane stress condition. In the present case, with  $\rho = 0.5$  or 0.9, ratio  $\epsilon_{\theta}/\epsilon_r$  is equal to 0.20 or 0.81, respectively, and these values are close to the experimental results shown in Figs. 6 and 7.

For  $\rho = 0.5$  (low value of the biaxial stress ratio), whereas the tangential strain is small and almost unchanged, the radial strain increases at the beginning of each step and then remains stabilized with subsequent cycles. In addition, the amount of strain accumulation during the accommodation period is more important with increasing applied load level. For  $\rho = 0.9$  (high value of the biaxial stress ratio), both radial and tangential strains have a similar behavior during cycling in terms of the strain accumulation before stabilization; this behavior could be expected, since both strains have almost the same magnitude for each step. For a given biaxial stress ratio, the effect of the temperature on the induced strains (radial and tangential strains) is quite small, as expected, since the test temperature is not high. For a higher temperature, this situation may be quite different and is presently under study.

### HYSTERESIS LOOPS

Typical stabilized hysteresis loops of the measured radial and tangential strains in terms of the applied load (constant load amplitude with  $R = 0$ ) are shown in Fig. 8 for tests at room temperature and in Fig. 9 for tests at 200°C. The hysteresis loops in Figs. 8(a) and 9(a) were obtained for a biaxial stress ratio equal to 0.5, whereas those in Figs. 8(b) and 9(b) correspond to a biaxial stress ratio of 0.9. It is seen that the radial strain hysteresis loops follow a smooth path, whereas this is not the case for the tangential strain hysteresis loops. This may be explained, in part, by the fact that the radial strain is directly given by one strain gage (oriented in the radial direction of the disk specimen), whereas the tangential strain is calculated on the basis of the three measured strains from the rosette.

These figures show that at the minimum load, the residual radial strain is more important than the residual tangential strain; this difference is more pronounced with a low value of the biaxial stress ratio. Moreover, the plastic component of the radial strain (width of the hysteresis loops) becomes more significant as the applied load increases. Nevertheless, under the test conditions considered here, the loop widths remain small as compared to the peak strain; this may be explained by the pseudoelastic state of the material under stabilized conditions. A similar behavior has already been observed by Yoshida,<sup>10</sup> who tested a stainless steel under biaxial cyclic

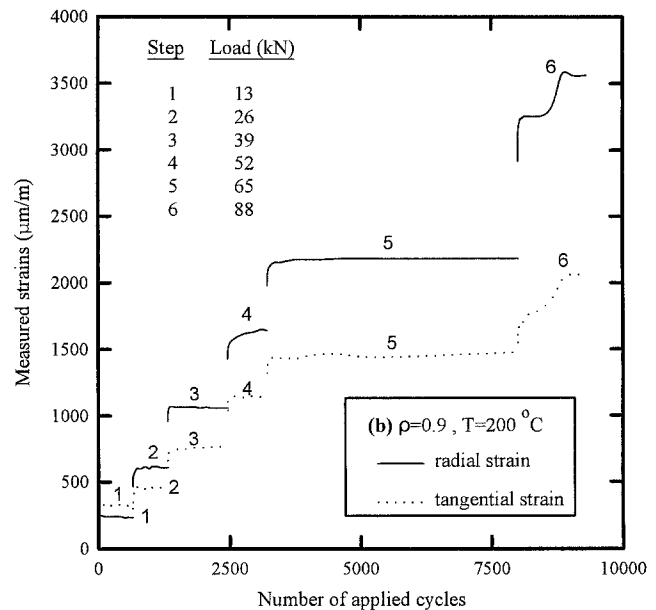
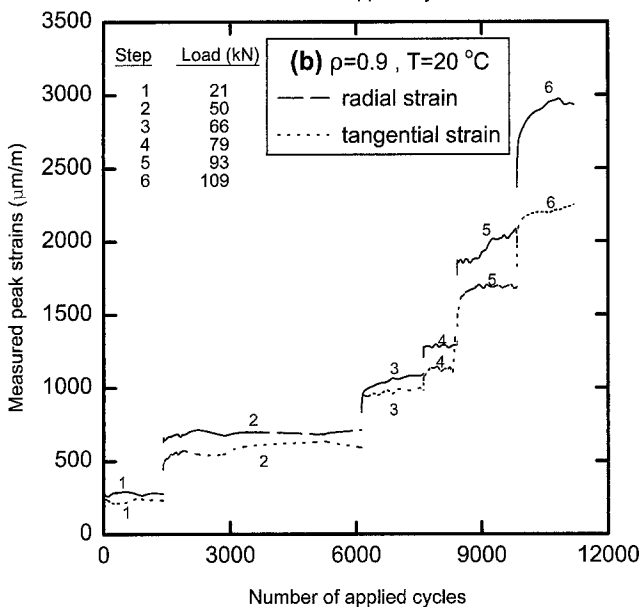
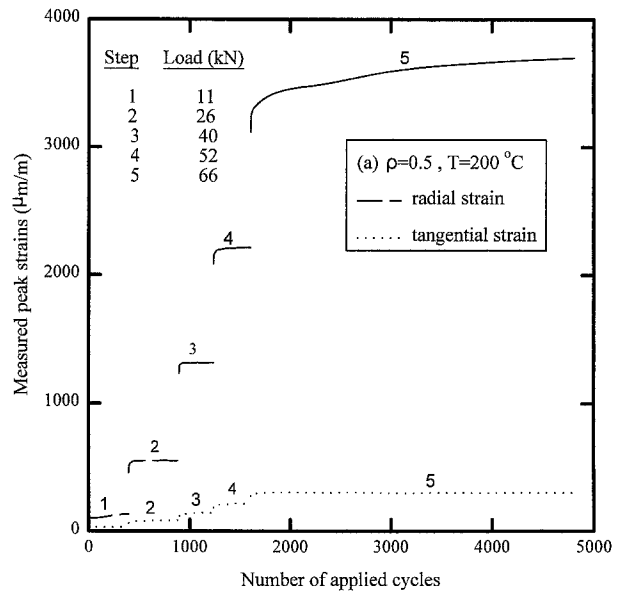
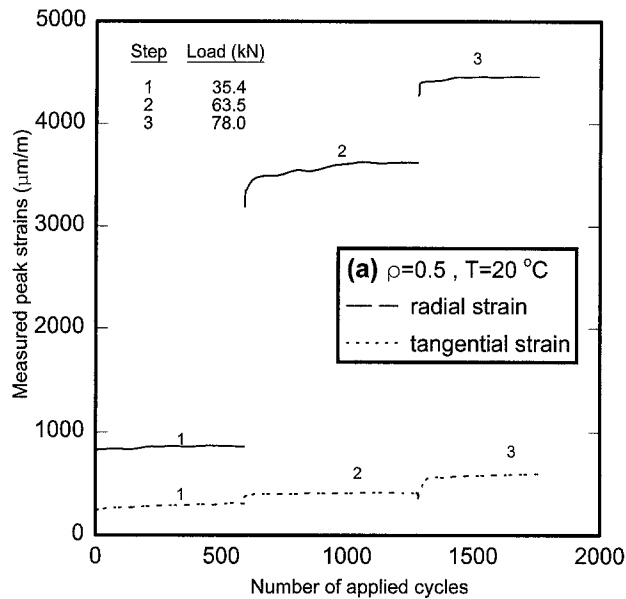


Fig. 6—Typical variation of peak strains during multistep tests at 20°C: (a)  $\rho = 0.5$ , (b)  $\rho = 0.9$

Fig. 7—Typical variation of peak strains during multistep tests at 200°C: (a)  $\rho = 0.5$ , (b)  $\rho = 0.9$

loading with a positive load ratio ( $R > 0$ ) using a cruciform specimen.

### Cyclic Stress-strain Representation

The Tresca and von Mises stress-strain equivalents are usually considered for reducing the biaxial cyclic stress-strain characteristics into an equivalent uniaxial behavior. The von Mises concept is related to the strain distortion energy, whereas the Tresca concept refers to the maximum shear stress. For each concept, the equivalent stress and strain are calculated on the basis of the measured stabilized strains for the specific loading conditions. In the present study, these calculations are performed as follows:

- The radial and tangential stresses in the test section are determined on the basis of the elastic components of the measured strains using generalized Hooke's law; the details are given in Appendix B. The elastic strain components are obtained from the hysteresis loop by

subtracting the residual strain (strain at zero load) and the plastic strain (width of the hysteresis loop) from the measured total strain (strain at maximum load). The equivalent von Mises and Tresca stresses [eqs (C1) and (D1), respectively] are then expressed in terms of the measured elastic component of the radial strain and the biaxial stress ratio.

- The elastic component of the strain in the direction perpendicular to the plane of the biaxial stress field (i.e.,  $\epsilon_z$ ) is computed on the basis of the Hooke's law with the assumption of the plane stress condition (Appendix B). The plastic component of this strain is computed under the assumption of volume constancy; in this condition, a Poisson's ratio equal to 0.5 is considered.
- With the stabilized stresses and strains obtained from calculations, equivalent elastic and plastic strains are

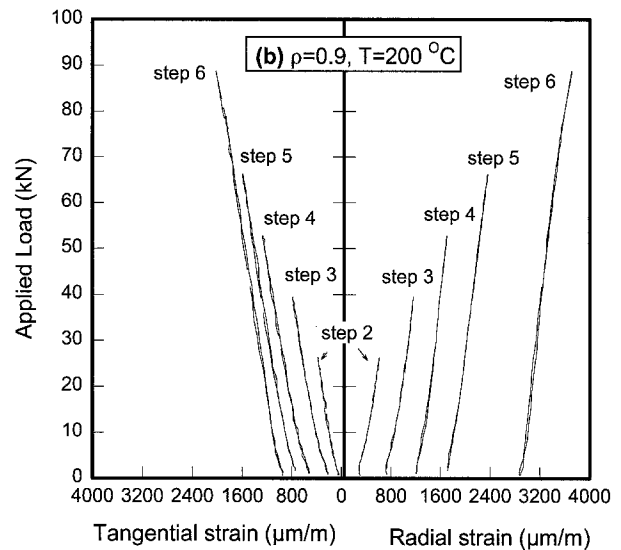
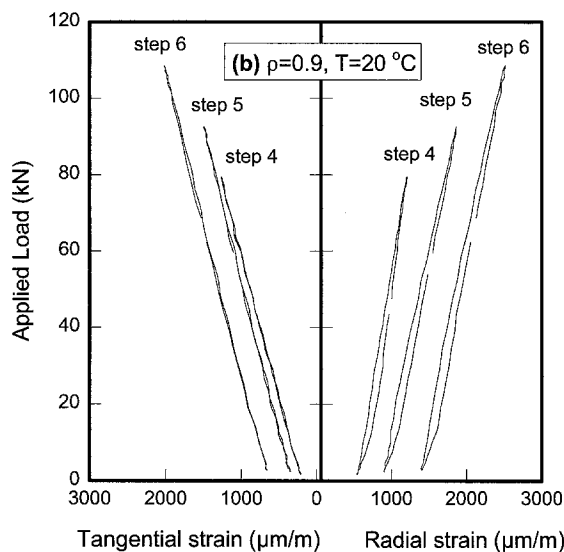
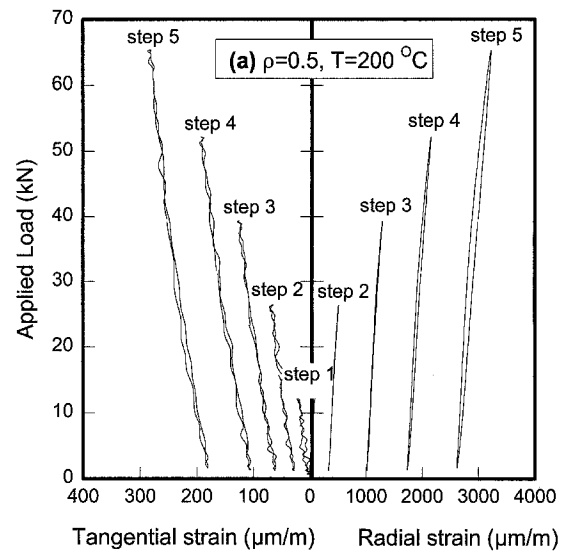
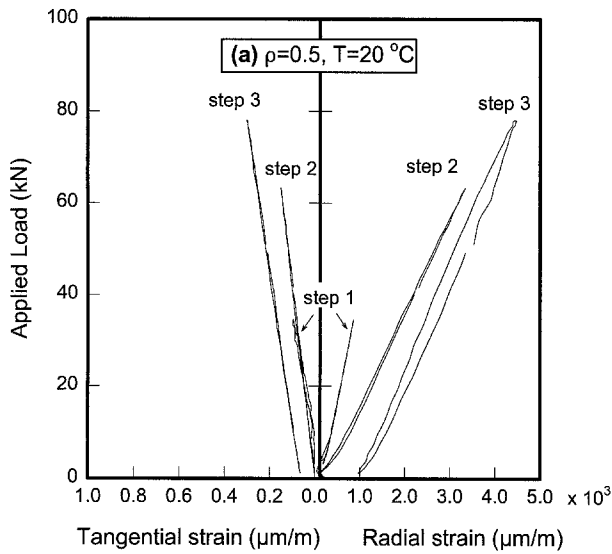


Fig. 8—Typical stabilized hysteresis loops of radial and tangential strains at 20°C: (a)  $\rho = 0.5$ , (b)  $\rho = 0.9$

Fig. 9—Typical stabilized hysteresis loops of radial and tangential strains at 200°C: (a)  $\rho = 0.5$ , (b)  $\rho = 0.9$

determined according to each concept. The detailed procedure is explained in Appendixes C and D.

- Overall von Mises and Tresca equivalent strains [eqs (C4) and (D4)], respectively are then defined as the sum of the elastic and plastic equivalent strains. The extension of the equivalent strain concept to the overall strain is commonly used,<sup>11</sup> since the overall strain reduces to the elastic strain under a low load level and is close to the plastic strain under a high load level. Thus, the use of an overall equivalent strain permits one to cover the transition zone in which the elastic and plastic strains are of the same order of magnitude. Consequently, the cyclic behavior for both elastic and plastic regions could be conveniently examined.

Figures 10 and 11 show the cyclic behavior of the material studied under four biaxial stress ratios on the basis of von

Mises and Tresca concepts, respectively. Also included in these figures is the conventional uniaxial cyclic stress-strain curve at room temperature; unfortunately, the uniaxial cyclic response at 200°C is not presently available, but it is expected that the deviation of this curve with respect to that at 20°C is small. The uniaxial cyclic curve was established on the basis of the maximum values of the cyclic stresses and cyclic strains and is different from the conventional curve using the amplitude values. Although the curves using strain and stress amplitudes describe a relatively consistent material behavior with respect to those established from maximum stresses and strains, the latter type of data representation is necessary in the design process of some particular components. It should be noted that residual stresses could have an influence on the calculated peak stresses, since they may affect the amplitude of the measured strains and, therefore, the amplitude of the calculated stresses.

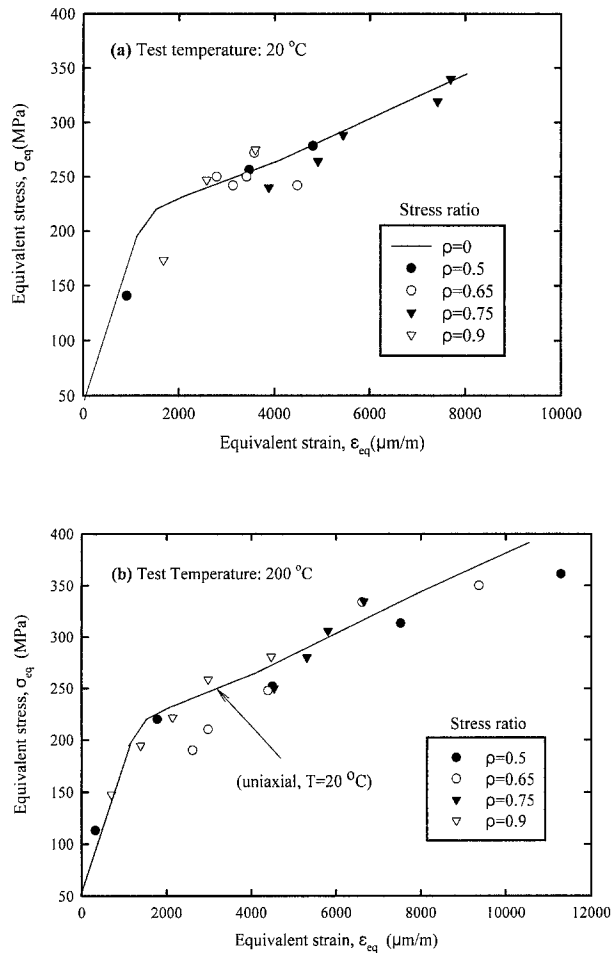


Fig. 10—Cyclic stress-strain behavior according to the von Mises concept: (a)  $T = 20^\circ\text{C}$ , (b)  $T = 200^\circ\text{C}$

With the von Mises concept, the biaxial cyclic stress-strain characteristic of the material under different biaxial tensile stress states may be reasonably represented by the uniaxial behavior for both test temperatures (Fig. 10) and at all strain levels. However, application of the Tresca concept is less successful; in particular, the deviation of the biaxial characteristic from the uniaxial cyclic response increases with an increase of the biaxial stress ratio and strain level.

### Discussion of the Cyclic Behavior

The effectiveness of the von Mises and Tresca concepts in reducing the biaxial stress states to an equivalent uniaxial stress state may be appreciated by looking at the overall deviation of the biaxial cyclic data from the uniaxial behavior. This deviation can be evaluated for each particular biaxial stress ratio as follows:

$$r = \sqrt{\frac{\sum_{i=1}^{i=N_e} (x_\rho^i - x_0^i)^2}{N_e}} \quad (1)$$

where  $x_\rho^i$  is the value of the equivalent von Mises (or Tresca) stress corresponding to a particular value of the equivalent

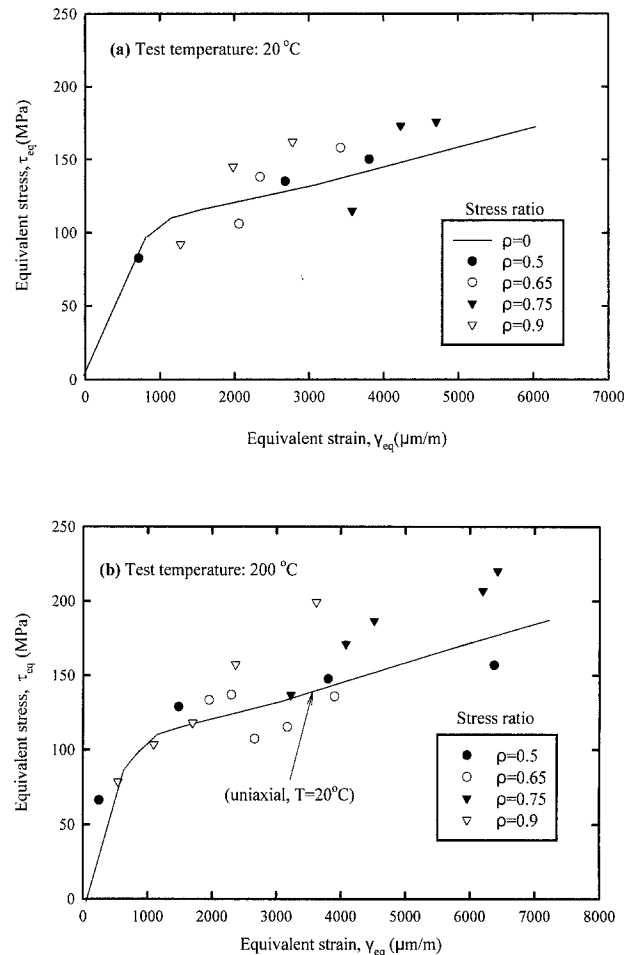


Fig. 11—Cyclic stress-strain behavior according to the Tresca concept: (a)  $T = 20^\circ\text{C}$ , (b)  $T = 200^\circ\text{C}$

von Mises (or Tresca) strain and  $x_0^i$  is the value of  $x_\rho^i$  associated with uniaxial loading condition;  $N_e$  is the total number of the cyclic stress-strain data obtained under the different biaxial stress states. Since only the room temperature uniaxial cyclic data are available,  $N_e$  is limited to the number of data used in the plot of the curves in Figs. 10a and 11a.

Although the number of data is small, it is seen from Fig. 12 that the deviation of the biaxial cyclic data increases significantly with an increase of the stress ratio in the case of the Tresca concept. With the von Mises concept, the same trend is also observed, but to a lesser extent. In particular, for  $\rho = 0.9$ , with the Tresca concept, the deviation is about 2.5 times that associated with the von Mises concept.

The relatively weak performance of the Tresca concept in establishing the biaxial-uniaxial correlation may be explained by the fact that it does not take into account the contribution of the in-plane minor principal stress and strain ( $\sigma_\theta, \epsilon_\theta$ ). In this study, these stress and strain components are of the same order of magnitude as compared to the in-plane major principal stress and strain ( $\sigma_r, \epsilon_r$ ). Figure 12 suggests that the von Mises concept is relevant for cyclic stress-strain data reduction from a biaxial stress state to the uniaxial case.

This type of data representation is very useful, since it contributes to the modeling approach of the stress-strain behavior necessary for any analytical or numerical stress analysis of mechanical components subjected to a cyclic biaxial tensile

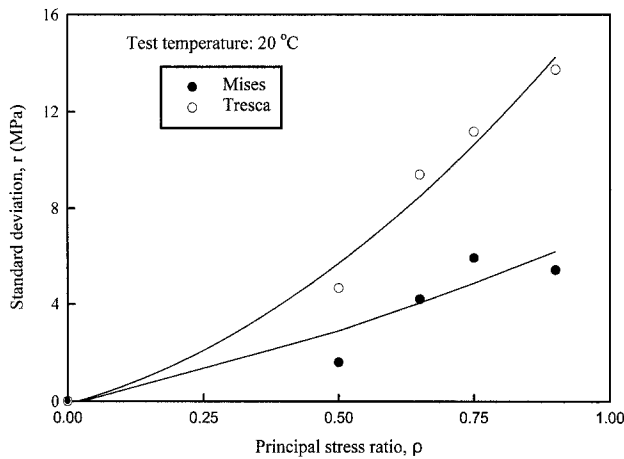


Fig. 12—Performance of the von Mises and Tresca concepts

stress state. Moreover, this approach is important for life prediction methodology; since the in-plane minor principal stress component ( $\sigma_\theta$ ) has a significant influence on the cyclic behavior, its influence on the fatigue life of the components would not be negligible. Thus, it is necessary to include this stress component in the formulation of the fatigue damage parameter. It is worth noting that several fatigue damage parameters proposed in the past ignore the contribution of this stress component. To overcome this deficiency, a new fatigue damage parameter taking into account the most important influencing factors, including the in-plane minor principal stress component, will be discussed in a forthcoming paper.

## Conclusion

The setup of a relatively simple apparatus has been completed for studying biaxial fatigue with positive stress ratios at moderately high temperatures. An annular disk specimen was used to generate a biaxial stress state with both principal stresses in tension. A wide range of positive stress ratios are imposed in the test section of the specimen by changing only the inner diameter of the disk. An experimental verification, carried out to evaluate the performance of the testing system, shows that the behavior of the test section of the specimen under axisymmetric loading is acceptable (within a strain deviation of 5 percent from the results obtained by finite element analysis).

Tests on Type-304 stainless steel disk specimens under biaxial multistep cycling at room temperature and at 200°C were carried out with four biaxial stress ratios (0.5, 0.65, 0.75 and 0.9). The results are analyzed together with those obtained under uniaxial cyclic loading, and the main conclusions are as follows: (i) for a high value of the biaxial stress ratio, the intermediate principal stress has an important effect on the cyclic stress-strain behavior and should be considered in establishing the cyclic characteristic of the material; (ii) the effect of the temperature on the cyclic behavior of the tested material is not conclusive, since the difference between the two considered test temperatures was relatively small; (iii) the von Mises concept appears to be more appropriate than the Tresca concept for reducing the biaxial cyclic stress-strain data to a single master curve, particularly at a high strain level. Further experimental investigation should be carried out to examine the validity of this statement for

other materials and/or loading conditions. This study shows that under a biaxial stress state with both principal stresses in tension, it is important to consider all principal stress and strain components in establishing the stabilized behavior of a material that is necessary for any reliable design procedure.

## Appendix A: Summary of the Principal Biaxial Testing Methods

On the basis of the biaxial stress ratio specification ( $\rho$  ratio between the in-plane minimum and maximum principal stresses  $\sigma_2$  and  $\sigma_1$ ), the experimental techniques may be classified into two categories: (1) tests using two or more independent loading systems and (2) tests using a single loading system. In the first category, the biaxial stress ratio is specified by the applied load magnitude, whereas in the second category, it depends on the specimen geometry or the loading fixture configuration.

Figures 13 and 14 summarize the principal techniques developed in the past for conducting biaxial testing with the possible range of the imposed biaxial stress ratio. Figure 13 shows examples from the first category: round bar under torsion bending (case a), thin-walled tube subjected to a combined loading such as tension-torsion, axial load pressurization and tension-torsion pressurization (cases b-d) and cruciform specimen under biaxial loading (case e). Figure 14 gives examples of the second category: bending test on cantilever beams (case a), bulge test of flat plate (case b), anticlastic bending (case c) and tests using special fixture (cases d-e). A detailed description of these methods may be found in Ref. 1.

This summary reveals that the relevant promising methods for conducting fatigue tests under biaxial tensile stress state are the thin-walled tube under tension and internal/external pressure, the cruciform specimen, the bulge test and the bending of a cantilever beam. The first two methods are the most commonly used even though they require complex and costly servohydraulic testing systems; a large variety of biaxial stress ratios may be imposed using these methods. However, the user of the cruciform specimen should determine with care the test section geometry over which a known uniform biaxial stress state is obtained and reduce to a low level the stress concentration at the corner fillets. Also, with the thin-walled tube as well as with the bulge test, the temperature level is limited by the properties of the pressurizing medium. On the other hand, the applicability of the cantilever beam test is limited by the range of the imposed biaxial stress ratio, the upper limit of this ratio being the value of the plastic Poisson's ratio.

## Appendix B: Stress and Strain Fields in the Test Section of the Disk Specimen

On the basis of a plane stress condition in the test section (i.e.,  $\sigma_z = \sigma_{rz} = \sigma_{\theta z}$ ) the radial and tangential stresses in this region are given by

$$\begin{aligned}\sigma_r &= \frac{1}{1-\nu\rho} E\epsilon_r^e \\ \sigma_\theta &= \frac{\rho}{1-\nu\rho} E\epsilon_r^e,\end{aligned}\quad (\text{B1})$$

where  $\epsilon_r^e$  is the elastic component of the measured radial strain. The elastic component of  $\epsilon_z$  is given by



Cases	Testing methods	Schematic representation	Stress ratio rang ( $\rho$ )
(a)	Round bar under torsion-bending		$-1 \leq \rho \leq 0$
(b)	<u>Thin-walled tube</u> under: Tension-torsion		$-1 \leq \rho \leq 0$
(c)	Tension-pressure		$0 \leq \rho \leq 1$
(d)	Tension-torsion pressure		$-1 \leq \rho \leq 1$
(e)	Cruciform specimen		$-1 \leq \rho \leq 1$

Fig. 13—Biaxial testing methods using two or more loading systems

$$\epsilon_z^e = \frac{-\nu(1 + \rho)}{1 - \nu \cdot \rho} \epsilon_r^e. \quad (B2)$$

The plastic strain component is obtained from the assumption of volume constancy:

$$\epsilon_z^p = -\epsilon_r^p - \epsilon_\theta^p, \quad (B3)$$

where  $\epsilon_r^p$  and  $\epsilon_\theta^p$  are the plastic radial and tangential strains that are determined from the width of the hysteresis loops. The total strain  $\epsilon_z$  is determined by adding the elastic strain

obtained from eq (B2) to the plastic strain obtained from eq (B3).

### Appendix C: von Mises Equivalents

The equivalent von Mises stress is obtained from the radial elastic strain component as follows:

$$\sigma_{eq} = \frac{\sqrt{1 - \rho + \rho^2}}{1 - \nu \cdot \rho} E \epsilon_r^e. \quad (C1)$$

On one hand, the von Mises equivalent of the elastic strain is given by

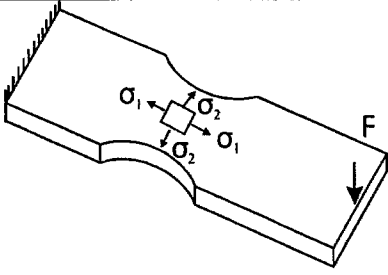
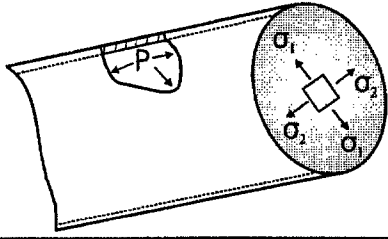
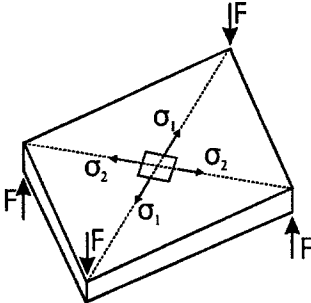
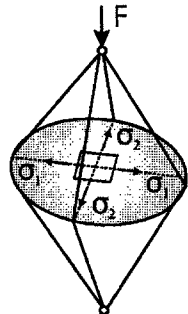
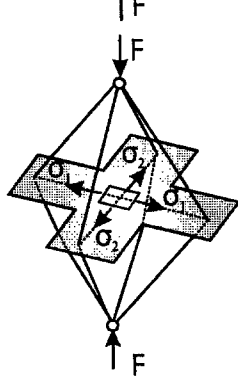
Cases	Testing methods	Schematic representation	Stress ratio rang ( $\rho$ )
(a)	Cantilever bending		$0 \leq \rho \leq 0.5$
(b)	Bulge test		$0 \leq \rho \leq 1$
(c)	Anticlastic bending		$-1 \leq \rho \leq 0$
(d)	<u>Special fixtures</u> Disc-shaped specimen under equibiaxial loading		$\rho=1$
(e)	Cruciform specimen with a spatial pantograph (for static loading)		$0 \leq \rho \leq 1$

Fig. 14—Biaxial testing methods using a single loading system

This work was sponsored by the Natural Science and Engineering Research Council (Grant bOGP 0038203) and by the Fonds pour la Formation des Chercheurs et l'Aide à la Recherche (Grant ER00276).

References

1. Zouani, A., Bui-Quoc, T., and Bernard, M., "A Proposed Device for Biaxial-tensile Fatigue Testing," *Fatigue and Fracture-1996*, ASME PVP-323, **1**, 331-339 (1996).
2. Ellyin, F. and Wolodko, J.D., "Testing Facilities for Multiaxial Loading of Tubular Specimens," *Proceedings of the 1995 Symposium on Multiaxial Fatigue and Deformation Testing Techniques*, SAE STP 1280, Denver, Colorado, 7-24 (1997).
3. Itoh, T., Sakane, M., Ohnami, M., and Socie, D., "Nonproportional Low-cycle Fatigue Criterion for Type-304 Stainless Steel," *ASME J. Eng. Mat. Tech.*, **117**, 285-292 (1995).
4. Brown, M.W. and Miller, K.J., "Biaxial Cyclic Deformation Behaviour of Steels," *Fatigue Eng. Mat. Struct.*, **1** (1), 93-106 (1979).
5. Doquet, V. and Pineau, M., "Multiaxial Low-cycle Fatigue Behaviour of Mild Steel," *Fatigue Under Biaxial and Multiaxial Loading*, ESIS10, ed. K. Kussmaul, D. McDiarmid and D. Socie, Mechanical Engineering Publications, London, 81-101 (1991).
6. Nishino, S., Hamada, N., Sakane, M., Ohnami, M., Matsumara, N., and Tokizane, M., "Microstructural Study of Cyclic Strain Hardening Behaviour in Biaxial Stress States at Elevated Temperature," *Fatigue Eng. Mat. Struct.*, **9**, 65-77 (1986).
7. Bonacuse, P.J. and Kalluri, S., "Elevated Temperature Axial and Torsional Fatigue Behavior of Haynes 188," *ASME J. Eng. Mat. Tech.*, **117**, 191-199 (1995).
8. Zouani, A., Bui-Quoc, T., and Bernard, M., "Optimal Design of a Disk-shaped Specimen for Biaxial-tensile Fatigue Testing," *ASTM J. Test. Eval.*, **24** (5), 287-294 (1996).
9. Murakami, S., Kawai, M., and Ohmi, Y., "Effects of Amplitude-history and Temperature-history on Multiaxial Cyclic Behavior of Type-316 Stainless Steel," *ASME J. Eng. Mat. Tech.*, **111**, 278-285 (1989).
10. Yoshida, F., "Uniaxial and Biaxial Creep-ratcheting Behavior of SUS 304 Stainless Steel at Room Temperature," *ASME Int. J. Pres. Ves. Piping*, **44**, 207-223 (1990).
11. Dowling, N.E., *Mechanical Behavior of Materials*, Prentice Hall, Englewood Cliffs, NJ, 536-540 (1993).

$$\epsilon_{eq}^e = \frac{\sqrt{1 - \rho + \rho^2}}{1 - \nu \cdot \rho} \epsilon_r^e \quad (C2)$$

On the other hand, the von Mises equivalent of the plastic strain is calculated with an assumption of the volume constancy condition (Poisson's ratio = 0.5):

$$\epsilon_{eq}^p = \frac{2}{\sqrt{3}} \sqrt{(\epsilon_r^p)^2 + (\epsilon_\theta^p)^2} + \epsilon_r^p \epsilon_\theta^p \quad (C3)$$

An overall equivalent strain is then defined as follows:

$$\epsilon_{eq} = \epsilon_{eq}^e + \epsilon_{eq}^p \quad (C4)$$

Appendix D: Tresca Equivalent

The equivalent Tresca stress is defined by

$$\tau_{eq} = \frac{1}{2(1 - \nu \rho)} E \epsilon_r^e \quad (D1)$$

On one hand, the Tresca equivalent of the elastic strain is calculated from

$$\gamma_{eq}^e = \frac{1 + \nu}{1 - \nu \rho} \epsilon_r^e \quad (D2)$$

On the other hand, the Tresca equivalent of the plastic strain is obtained on the basis of the volume constancy condition:

$$\gamma_{eq}^p = \epsilon_r^p + \frac{\epsilon_\theta^p}{2} \quad (D3)$$

Finally, an overall equivalent strain is defined as follows:

$$\gamma_{eq} = \gamma_{eq}^e + \gamma_{eq}^p \quad (D4)$$